Proceedings of ERAD (2004): 99–104 © Copernicus GmbH 2004

ERAD 2004

The structure and variability of tropical oceanic precipitation in the western Pacific warm pool and eastern Pacific ITCZ

S. E. Yuter

University of Washington, Seattle, Washington, USA

Abstract. Geosynchronous and low-earth-orbiting satellite data and ship-based C-band radar data obtained for precipitating storms within the western Pacific warm pool (longitude 156° E) and the eastern Pacific ITCZ (longitude 125° W) are analyzed to determine 3D characteristics of precipitation structure. Beneath cloud top, the differences in radar-derived characteristics between smaller versus larger precipitation systems for a given region are much greater than differences between precipitation systems of similar size in the W Pacific versus E Pacific. Convective and stratiform precipitation regions within larger precipitation areas are usually more vigorous, with stronger precipitation growth and near surface reflectivity, than their counterparts within smaller, more isolated precipitation. Regional differences in the relative frequency of small versus large area precipitation systems contribute to differences in regional average precipitation characteristics.

1 Introduction

The location, intensity, structure, and duration of precipitating systems are important for understanding the global water cycle and for the initialization and evaluation of global forecast models. Over the Pacific, open-ocean precipitation has two local maxima. One maximum is over the western Pacific warm pool, centered near 2° S and 156° E, and peaks during December-February. The other maximum is over the eastern Pacific ITCZ, centered near 8° N, 125° W and peaks during June–August. The characteristics of precipitation and the associated latent heat release in these two regions have ramifications for large-scale atmospheric circulations.

Characterization of precipitation structure over the open ocean using satellite data has several limitations. Geosynchonous IR brightness temperatures represent an indirect proxy for precipitation structure underneath. Low-earth orbiting sensors such as the TRMM satellite's K_u-band Precipitation Radar (PR) provide direct information on the 3D reflectivity structure of precipitation, but physical interpretation of the TRMM PR data is complicated by a narrow swath width, poor temporal sampling, a minimum sensitivity of ∼18 dBZ, and attenuation in rain (Kummerow et al., 1998). Field-project shipborne radar data sets sample with high sensitivity and high time resolution for a period of weeks but may not be representative of long-term climatology. In this study, combined analysis of field project and satellite radar data is used to counterbalance weaknesses of the individual data sets.

Correspondence to: S. E. Yuter
(yuter@atmos.washington.edu)

2 Examination of observations from two tropical oceanic field projects

Shipborne C-band radar data obtained during two open-ocean field experiments, TOGA COARE in the western Pacific (Short et al., 1997) and TEPPS in the eastern Pacific (Yuter and Houze, 2000) are examined in conjunction with geosynchronous satellite data (Table 1). The shipborne radar data were processed to minimize differences related to the different equipment and radar scan strategies employed during the two experiments. The radar domain used in this study extends between 15–83 km range from the ship. Automated quality control is used to remove sea clutter. The polar-coordinate data are interpolated to a 2 km Cartesian grid in the vertical and horizontal using NCAR REORDER with the lowest layer between 2 km and 4 km altitude. A classification based on reflectivity threshold and texture is applied to objectively identify convective precipitation (CONV), stratiform precipitation (SF), weak non-precipitating echo (<15 dBZ), and regions without echo within the lowest layer of each interpolated volume (Yuter and Houze, 1997).

The frequency distribution of low-level precipitation region size (CONV area + SF area) within the 166 km diameter radar domain is roughly log-normal for both COARE and TEPPS (not shown). During COARE, precipitation area

Table 1. Geosynchronous IR satellite and shipborne C-band radar data sample characteristics. Radar domain is area between circles of 15 km and 83 km radius.

Characteristic	TOGA-COARE	TEPPS
Study Area	West Pacific Warm Pool	East Pacific ITCZ
Field Study Period	Nov. 1992 - Feb. 1993	Aug. 1997
Satellite IR data	1 hourly (GMS)	3 hourly (GOES)
Total Ship Radar Volumes	10,057	4605
Radar Echo Area > 20% of domain	994 volumes	1098 volumes
Radar Echo Area > 40% of domain	341 volumes	256 volumes
Radar Echo Area > 1% and < 20% of domain	5497 volumes	2561 volumes

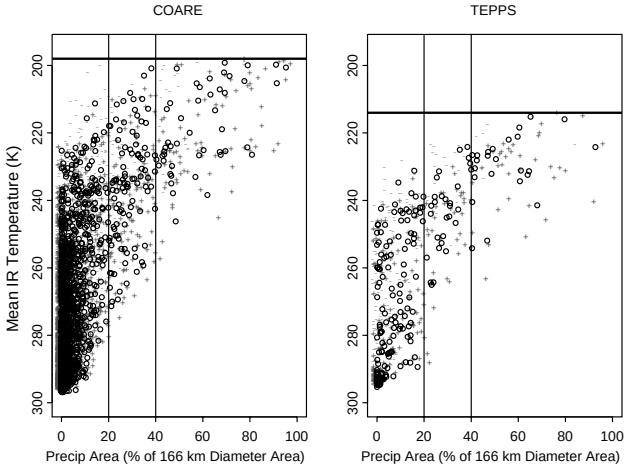

Fig. 1. Scatter plots of total precipitation area versus mean geosynchronous IR temperature over the 166 km diameter radar domain centered on the ship location. Time difference between IR data and radar volumes is no more than 15 minutes. Three estimates of precipitation area are shown corresponding to calibration offsets of 0 dB (circles), +5 dB (+) and −5 dB (−). Left panel – COARE: 1681 satellite-radar pairs. Right panel – TEPPS: 192 pairs.

>1% of the radar domain was observed 65% of the time as compared to 80% for TEPPS (Table 1). Although the projects were of different duration, the number of samples containing precipitation area >20% of the radar domain area are similar.

IR and passive microwave satellite data yield different maps of precipitation across the Pacific. Surface-based radar can help resolve ambiguities in satellite data physical interpretation. Figure 1 shows scatter plots of precipitation area versus mean IR temperature over the 166 km diameter radar domain. To address potential errors related to the relative radar calibration uncertainty between the field projects, precipitation area is estimated using three calibration offsets for each radar volume. The TEPPS plot resembles a vertically-compressed version of the COARE plot. Minimum average IR temperatures are 198 K in COARE as compared to 214 K in TEPPS. The underlying surface-radar-defined precipitation areas extend up to 100% of the radar domain during both projects.

Radar echo-top data can be used to assess the vigor of precipitating storms. Higher radar echo tops are associated with storms with higher convective available energy and stronger updrafts. A robust echo-top statistic between field project data sets must take into account several potential confounding factors such as the non-Gaussian distribution of echo-top height, incomplete beamfilling, and differences in radar calibration, sensitivity, and scan strategy. To mitigate these factors, an echo top height index is defined corresponding to highest layer in the Cartesian interpolated volume that contains at least 25% of the echo area relative to the layer with the volume's largest echo area (usually the lowest layer).

Figures 2a and b compare the distribution of echo top height index as a function of precipitation area for volumes with area >40% of the radar domain during COARE and TEPPS. The distribution mode (darkest grid boxes) for both is between 10 and 12 km altitude. COARE has a higher frequency of volumes with echo-top height indices between 12 to 14 km altitude than TEPPS, but this cannot account for the 16 K difference in minimum average IR temperature. Figures 2c and d illustrate characteristics of precipitation areas >1% and <20% of the radar domain. In this case, modal echo-top heights are between 6 and 4 km altitude for both COARE and TEPPS. Small precipitation areas between 1% and 5% area can have a range of echo tops up to 14 km (Figs. 2c, d). The distribution is skewed to higher altitudes for both regions. Examination of echo-top height index versus area for the convective precipitation subsets (Fig. 3) yields an analogous picture. Modal echo tops are similar between CONV subsets within large precipitation areas and are systematically lower for small precipitation areas. The cloud-filled column between the radar echo top and the IR-defined cloud top can be inferred to contain only small, non-precipitating particles as the echo is too weak to be sensed by the shipborne C-band radars (<0 dBZ). The relative vigor of W versus E Pacific large precipitating storms is identical in the distribution mode, but the W Pacific has some stronger outliers.

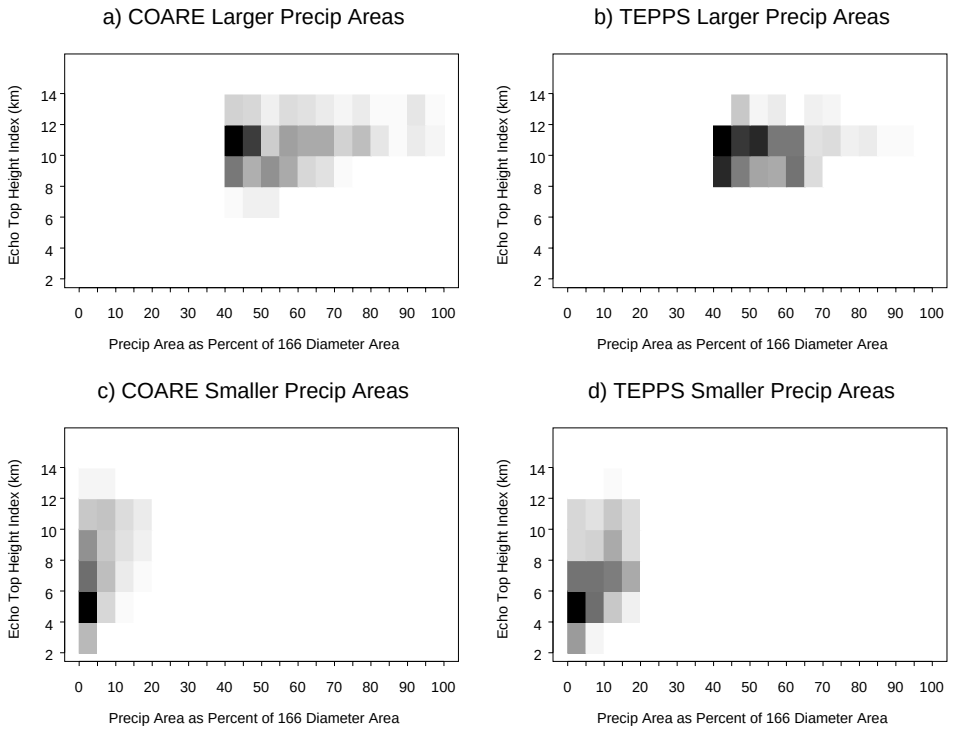

Fig. 2. Frequency distribution of precipitation area versus echo top height index. Darker colors correspond to higher frequencies. Large precipitation areas are the subset of volumes with precipitation area $\geq$40% of the radar domain area. Small precipitation areas are the subset of volumes with precipitation area $>$1% and $<$ 20% of the radar domain area.

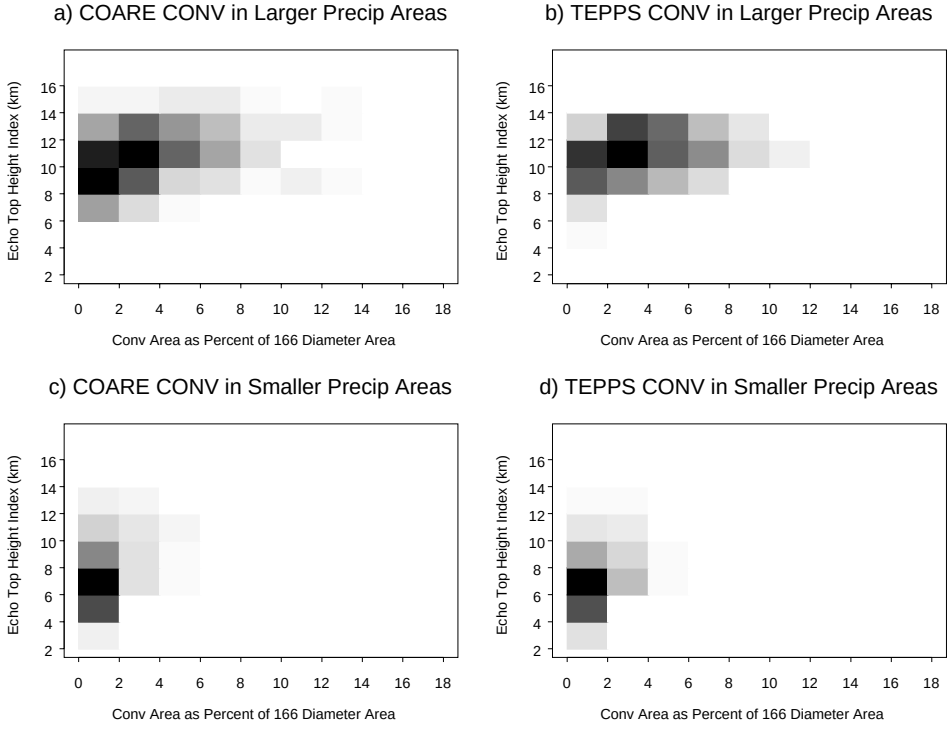

Fig. 3. As in Fig. 2 except frequency distribution of convective precipitation area vs. echo top height index over convective precipitation areas.

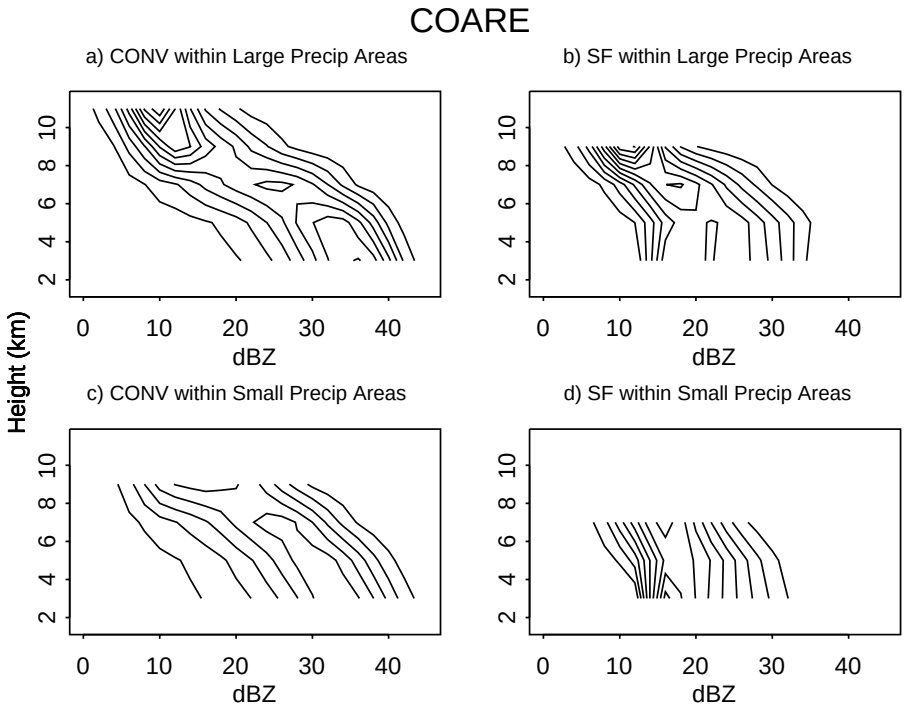

Fig. 4. Accumulated CFADs of radar reflectivity from COARE for a) convective and b) stratiform precipitation subsets of large precipitation areas >40% of radar domain (341 volumes) and for c) convective and d) stratiform precipitation subsets of small precipitation areas >1% and <20% of radar domain (5497 volumes).

Several characteristics of the vertical structure of the precipitating regions in the W and E Pacific are revealed in accumulated contoured frequency by altitude diagrams (CFADs, Yuter and Houze, 1995) shown in Fig. 4. CFADs were calculated using data within the interior of echoes to limit the impact of incomplete beamfilling and differences in scan strategy between the two projects. For convective precipitation regions within large precipitation areas (Fig. 4a) there is a distinct trend of increasing Z with decreasing altitude through the 0°C level at 5 km (4 km to 6 km layer) indicating precipitation growth within both the ice and rain regions of the storm. The stratiform CFAD for large precipitation areas (Fig. 4b) shows precipitation growth within the ice region above 5 km altitude but the nearly vertical trend of Z below 5 km altitude indicates little to no growth in the rain regions. The CFAD for convective precipitation within small precipitation regions (Fig. 4c) has a wider distribution of Z at each level and the mode of the CFAD is shifted to lower Z values compared to Fig 4a. The reflectivity mode at the surface is 3 dB lower for convective precipitation within smaller areas. The mode of stratiform CFAD for small precipitation areas (Fig. 4d) indicates little to no precipitation growth through the depth of the radar echo and a near-surface reflectivity mode 6 dB less than its large precipitation counterpart (Fig. 4b and d).

Examination of CFADs for TEPPS (not shown) reveals nearly identical frequency distribution patterns and slightly smaller relative dBZ offsets between near-surface reflectivity in convective and stratiform components of large versus small precipitation areas. Precipitation structures are similar for precipitation systems of similar sizes in both W and E Pacific, but there are large differences in structure between large and small precipitation areas for a given region.

3 Analysis of TRMM Precipitation Radar data

The TEPPS data were obtained during the 1997 El Nino event. The average SST in the TEPPS region was 1°C warmer than the previous non-El Nino year. Since the SST constrains the maximum temperature and humidity of the atmosphere just above the ocean surface, the energy available for convection during TEPPS was higher than during a typical August. The representativeness of the TEPPS data set for the E Pacific rests on how this difference in available energy is manifested. Between El Nino and non-El Nino years, storms in the E Pacific could be on average stronger, more numerous, neither, or both. To examine this issue, TRMM satellite PR data for a 6° latitude by 4° longitude box centered on the TEPPS study area in the E Pacific from the month of August during the non-El Nino years of 1998, 1999, and 2000 are examined and compared to data for a box in the W Pacific centered on the COARE study area obtained during December for the same years.

Table 2 provides some statistics on the frequency of all types of precipitation within the W and E Pacific boxes. The probability of precipitation within the TRMM PR sample is

Table 2. West and east Pacific TRMM PR sample characteristics. Uncertainty (±) is standard deviation of distribution. Rain area is computed using PR "rain certain" pixels. Orbit swaths refer to subset of full orbit data within 6°×4° boxes centered on the field project areas.

Data Set	# Orbit Swaths	% Rain Area of Swath Area	% SF Area of Rain Area
West Pacific All	124	7.4 %	76±17%
East Pacific All	127	8.1 %	89±9%

Table 3. Characteristics of TRMM PR-sampled large area precipitation regions. % of Total refers to large precipitation region sample compared to all PR sampled precipitation.

Data Set	# Orbit Swaths	% of Total Rain Area	% of Total CONV Area	% SF Area of Rain Area
West Pacific Large Area	23	67 %	56%	80±10%
East Pacific Large Area	36	78 %	78%	87±8%

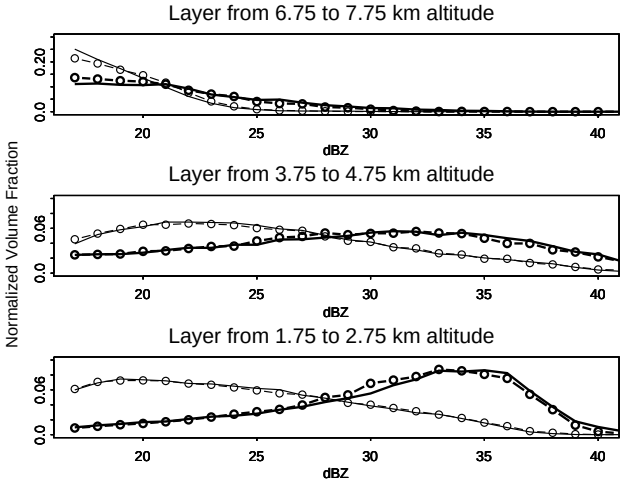

Fig. 5. Frequency distributions of TRMM PR observed reflectivity at three different altitudes for 3 month data sets over 6° latitude by 4° longitude regions centered on field project areas. W Pacific data (solid lines) from December 1998, 1999, and 2000. E Pacific data (lines with circles) from August 1998, 1999, and 2000. Data are partitioned into convective (thicker lines) and stratiform (thinner lines) subsets. Top panel–ice layer from 6.75 to 7.25 km altitude. Middle panel – mixed phase layer from 3.75 to 4.75 km altitude. Bottom panel – rain layer from 1.75 to 2.75 km altitude.

slightly higher in the E Pacific (8.1%) as compared to the W Pacific (7.4%). Similar to the findings of Berg et al. (2002) for the December 1999–February 2000 period, the stratiform area fraction of the total precipitation area is larger in the E Pacific than the W Pacific.

The subset of data corresponding to larger precipitation features (defined for the TRMM PR data as precipitation areas $>10\,000\,\mathrm{km}^2$ within an individual orbit swath intersecting the 6°×4° box) are examined in Fig. 5 and Table 3. Frequency distributions of PR reflectivity within convective and stratiform precipitation for three different altitude layers are nearly identical for the E and W Pacific storms indicating the similarity of their structures (Fig. 5). Large precipitation features make up a larger percentage of the total rain area in the E Pacific (78%) versus the W Pacific (67%) indicating a higher frequency of larger precipitation systems in the E Pacific (also shown in the field project data in Table 1). The higher probability of larger storms in the E Pacific is correlated with surface southerly wind events associated with 3–6 day easterly waves (Serra and Houze, 2002). Over three-quarters of the convective precipitation area in the E Pacific is associated with larger precipitation areas as compared with just over half for the W Pacific. These values indicate regional differences in the relative frequency distribution of small versus large precipitating systems and a greater relative importance of smaller precipitation systems to precipitation totals and heating in the W Pacific. The stratiform area fractions for large precipitation systems for the E and W Pacific are higher in the E Pacific but within one standard deviation of each other.

4 Conclusions

Satellite data and ship-based C-band radar obtained for precipitating storms within the western Pacific warm pool (longitude 156° E) and in the eastern Pacific ITCZ (longitude 125° W) are analyzed. A significant difference between the regions is the relation of surface precipitation area to the IR temperature of the overlying cloud (Fig. 1). For the same range of precipitation area sizes, minimum average cloud top temperatures are 16° C lower in the west Pacific as compared to the east Pacific. The tallest echo-top height indices extend higher in W Pacific than E Pacific, but the modal echo-top height indices are similar between the E and W Pacific indicating that the layer between radar echo top and cloud top

usually consists of cloud particles that too small to be observed by the shipborne C-band radar (Figs. 2 and 3).

Common to the E and W Pacific are structural differences between convective and stratiform regions that are part of larger versus smaller precipitation areas. Modal radar echo tops are 6 km higher and near-surface reflectivities are 2–3 dB stronger for convective cells within larger as opposed to smaller precipitation areas (Figs. 2, 3, and 4). Tropical oceanic small-area versus large-area precipitating systems have different structures. Larger precipitating systems have associated mesoscale circulations that act to increase the vigor of both convective and stratiform precipitation regions in terms of modal radar echo-top height, precipitation growth, and near-surface reflectivity compared to convective and stratiform regions within smaller precipitating systems without attendant mesoscale circulations.

For spatial scales up to 166 km, the differences in characteristics between smaller versus larger precipitation systems for a given region are much greater than differences between large precipitation systems in the E Pacific versus W Pacific (Fig. 5). This study confirms the importance of precipitation area as a key discriminator among precipitation structures (Nesbit et al., 2000) and the multimodal frequency distribution of tropical oceanic radar echo tops (Johnson et al., 1999). These results imply that simple grid box averages of tropical oceanic precipitation characteristics (e.g. Berg et al., 2002) may primarily reflect regional differences in the relative frequency of the modes rather than differences in the structure of precipitation within a mode.

References

Berg, W., et al.: Differences between east and west Pacific rainfall systems, J. Climate, 15, 3659–3672, 2002.

Johnson, R. H., et al.: Trimodal characteristics of tropical convection, J. Climate, 12, 2397–2418, 1999.

Kummerow, C., et al.: The Tropical Rainfall Measuring Mission (TRMM) sensor package, J. Atmos. Ocean. Tech., 15, 809–817, 1998.

Nesbit, S. W., et al.: A census of precipitation features in the tropics using TRMM: Radar, ice scattering and lightning observations, J. Climate, 13, 4087–4106, 2000.

Serra, Y. L. and Houze Jr., R. A.,: Observations of variability on synoptic time-scales in the east Pacific ITCZ, J. Atmos. Sci., 59, 1723–1743, 2002.

Short, D. A., et al.: Shipboard radar rainfall patterns within the TOGA COARE IFA, Bull. Amer. Meteor. Soc., 78, 2817–2836, 1997.

Yuter, S. E. and Houze Jr., R. A.: Three-dimensional kinematic and microphysical evolution of Florida cumulonimbus, Part II: Frequency distributions of vertical velocity, reflectivity, and differential reflectivity, Mon. Wea. Rev., 123, 1941–1963, 1995.

Yuter, S. E. and Houze Jr., R. A.: Measurements of raindrop size distributions over the Pacific warm pool and implications for Z-R relations. J. Appl. Meteor., 36, 847-867, 1997.

Yuter, S. E. and Houze Jr., R. A.: The 1997 Pan American Climate Studies Tropical Eastern Pacific Process Study. Part I: ITCZ Region, Bull. Amer. Meteor. Soc., 81, 451–481, 2000.